Graphene bilayer field-effect phototransistor for terahertz and infrared detection

V. Ryzhii* and M. Ryzhii
Computational Nanoelectronics Laboratory, University of Aizu, Aizu-Wakamatsu 965-8580, Japan
and Japan Science and Technology Agency, CREST, Tokyo 107-0075, Japan
(Received 22 January 2009; revised manuscript received 27 May 2009; published 16 June 2009)

A graphene bilayer phototransistor (GBL-PT) is proposed and analyzed. The GBL-PT under consideration has the structure of a field-effect transistor with a GBL as the channel sandwiched between the back and the top gates. The positive bias of the back gate creates the conducting source and drain sections in the channel, while the negatively biased top gate provides the potential barrier which is controlled by the charge of the photogenerated holes. The features of the GBL-PT operation are associated with the variation in both the potential distribution and the energy gap in different sections of the channel when the gate voltages change. Using the developed GBL-PT device model, the spectral characteristics, dark current, responsivity, photoelectric gain, and detectivity are calculated as functions of the applied voltages, energy of incident photons, intensity of electron and hole scattering, and geometrical parameters. It is shown that the GBL-PT spectral characteristics are voltage tuned. The GBL-PT performance as a photodetector in the terahertz and infrared regions of the spectrum can markedly exceed the performance of other photodetectors.

DOI: 10.1103/PhysRevB.79.245311 PACS number(s): 73.50.Pz, 73.63.−b, 81.05.Uw

I. INTRODUCTION

At present, infrared detectors are mostly based on narrow-gap semiconductors utilizing interband transitions. Technologies utilizing HgCdTe and InSb are well developed for infrared detection and imaging.[1,2] The necessity of further extension of the wavelength range covered by photodetectors and imaging devices on their base, widening of their functionality, as well as cost reduction in the production by using a mature processing technology has stimulated the development of quantum-well infrared photodetectors (QWIPs) based on A_3B_5 compound systems and SiGe alloys, utilizing intersubband (intraband) transitions (see, for instance, Refs. 2 and 3). Quantum-dot and quantum-wire infrared photodetectors (QDIPs and QRIPs) were proposed[4,5] and realized by many groups. The utilization of graphene layers and graphene bilayers,[6,7] opens up real prospects in the creation of novel photodetectors. The most important advantage of graphene relates to the possibility to control the energy gap in a wide range by patterning the graphene layer into an array of narrow strips (nanoribbons).[8,9] The energy gap in graphene bilayers can be varied by the transverse electric field[10–13] in different gated heterostructures. The graphene-based photodetectors can exhibit relatively high quantum efficiency (due to the use of interband transitions) and can be easily integrated with silicon readout circuits. A photodetector for THz and far-infrared (FIR) radiation based on a field-effect-transistor structure with the channel consisting of and array of graphene nanoribbons was proposed and analyzed recently.[14] In this paper, we discuss the concept of a THz/FIR photodetector with the structure of a field-effect transistor with a graphene bilayer as the device channel and photosensitive element. Using the developed device model, we calculate and analyze the detector characteristics. We demonstrate that such a graphene bilayer phototransistor (GBL-PT) can operate as a very sensitive and voltage tunable THz/FIR photodetector at elevated temperatures.

II. MODEL

The GBL-PT under consideration has a structure shown schematically in Fig. 1(a). The GBL channel is supplied with the source and the drain contacts and separated by a dielectric layer from the back gate. The latter provides the formation of a two-dimensional electron gas in the channel when the back gate is biased positively with respect to the source and the drain: $V_b > V_d > 0$. There is a top electrode serving as the top gate which is biased negatively ($V_t < 0$). Here, V_b, V_t, and V_d are the back-gate, top-gate, and source-drain voltages, respectively. The negative bias of the top gate results in a depletion of the section of the channel beneath the top gate (which in the following is referred to as the gated section). This partitions the channel into two highly conducting sec-

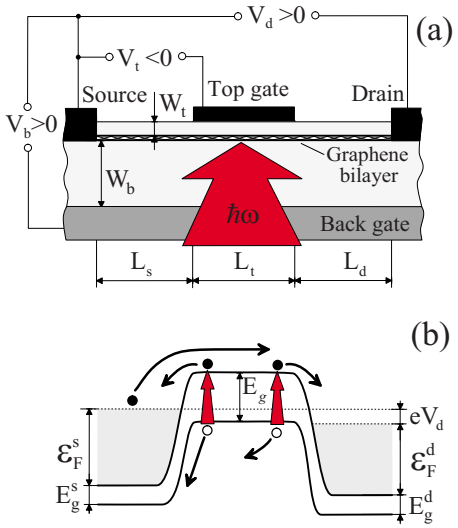

FIG. 1. (Color online) Schematic view of (a) a GBL-PT structure and (b) its band diagrams at bias voltages. Dark arrows indicate directions of electron (opaque circles) and holes (open circles) propagation.

tions (source and drain sections) and the depleted gated section. In the gated section, the potential barrier for electrons is formed. This barrier controls the injected electron current from the source to the drain. The GBL-PT band diagram under the bias voltages corresponding to the operation conditions is shown in Fig. 1(b). We assume that the back and the top gates are sufficiently transparent for the incoming radiation. The GBL-PT operation is associated with the variation in the source-drain electron current under illumination when the electron-hole pairs are generated in the depleted section. The photogenerated electrons are swept out to the conducting sections, whereas the photogenerated holes accumulated in the depleted section result in lowering of the potential barrier for the injected electrons. As shown below, the variation in the injected electron current can substantially exceed the current created by entirely photogenerated electrons and holes, so GBL-PTs can exhibit large photoelectric gain.

We consider the situation when the gated section is fully depleted. It occurs when $V_{th}^{*}<V_t<V_{th}$, where $V_{th}^{*}<V_{th}<0$ are the threshold voltages.[15] For a given back-gate voltage V_b, the threshold voltage V_{th} corresponds to the top-gate voltage V_t at which the bottom of the conduction band in the gated section aligns with the Fermi level in the source section, whereas V_{th}^{*} corresponds to the top-gate voltage at which the top of the valence band in the gated section aligns with the Fermi level in the source section. Figure 1(b) shows the GBL-PT band diagram corresponding just to the voltage range $V_{th}^{*}<V_t<V_{th}$ in the partial case when the Fermi level in the source section lie slightly above the top of the valence band in the gated section with the latter top approximately aligned with the Fermi level in the drain section (due to the pertinent value of V_d). The heights of the potential barrier induced in the gated (depleted due to $V_t<V_{th}$) section by the top-gate voltage (in the absence of illumination) for the electrons in the source and drain sections, Δ_0^s and Δ_0^d, are given by[15]

$$\Delta_0^s=-\frac{e(V_b+V_t)}{2},\quad \Delta_0^d=-\frac{e(V_b+V_t)}{2}-\varepsilon_F^s+\varepsilon_F^d+eV_d, \tag{1}$$

where ε_F^s and ε_F^d are the Fermi energies of electrons in the source and the drain sections, respectively. Equation (1) is valid only when $V_t<V_{th}$, so that $\Delta_0^s>\varepsilon_F^s$ and the gated section is depleted. If $V_{th}<V_t$, the electron charge in the gated section affects the barrier height Δ_0^s and the latter is given by a more complex formula (see Ref. 15). Since the electrons in the source and the drain sections are electrically induced, the pertinent electron Fermi energies are functions of V_b and V_b-V_d, respectively: $\varepsilon_F^s=\varepsilon_F^s(V_b)$ and $\varepsilon_F^d=\varepsilon_F^s(V_b-V_d)$. The energy gaps in the source, gated, and drain sections of the GBL channel, E_g^s, E_g, and E_g^d, are given by the following linear dependences relating the energy-gap values and the gate voltages (in line with Refs. 11, 13, and 16):

$$E_g^s=\frac{eV_bd}{2W},\quad E_g=\frac{e(V_b-V_t)d}{2W},\quad E_g^d=\frac{e(V_b-V_d)d}{2W}, \tag{2}$$

whereas the threshold voltages are, by definition and in line with Eq. (1), as follows:

$$V_{th}=-V_b-2\varepsilon_F^s/e,\quad V_{th}^{*}=-V_b-2(\varepsilon_F^s+E_g)/e. \tag{3}$$

Here d is a phenomenological parameter which accounts for the effect of partial screening of the external electric field and W is the thickness of the dielectric layers separating the GBL and the gates (which are set equal to each other: $W_t=W_b=W$). The linear voltage dependences given by Eq. (2) are valid when $E_g^s,E_g,E_g^d<\gamma_1$,[13,16] where $\gamma_1\simeq 0.4$ eV is the band parameter. In the case of photodetectors for THz/FIR radiation detection, the required values of the energy gap well satisfy this inequality. Actually, due to screening effects, the quantity d can be slightly different in the sections with high electron density (source and drain sections) and in the depleted section (gated section). In the following, we shall neglect such a difference setting in numerical estimates $d\sim d_0$, where d_0 is the spacing between the graphene layers in the GBL. This is justified by the fact that the values of the energy gaps in the source and the drain sections do not affect the GBL-PT characteristics essentially. In contrast, the quantity d in the gated section is one of the factors determining the energy gap which, in turn, determines the edge of the radiation absorption. However, the screening in the gated section is weak due to its depletion, so that the electron density as well as the hole density (under weak illumination) in this section are small; hence, $d\sim d_0$. If the electron system is degenerate but the Fermi energy in the source and the drain sections corresponds to the energy range where the GBL density of states can be considered as a linear function (disregarding the divergence at the conduction-band bottom), one obtains $\varepsilon_F^s\simeq eV_b(a_B/8W)$ and $\varepsilon_F^d\simeq e(V_b-V_d)(a_B/8W)$, so that $V_{th}\simeq -V_b(1+a_B/4W)$ and $V_{th}^{*}\simeq -V_b(1+a_B/4W+2d/W)$.[15] Apart from this, $\Delta_0^d\simeq\Delta_0^s+(1-a_B/8W)eV_d$. These approximations will be used in some (not all) final expressions. Here $a_B=k\hbar^2/me^2$ is the Bohr radius, k is the dielectric constant, m is the effective mass of electrons (and holes) in the GBL, and $\hbar$ is the Planck constant. One can see that $E_g^{s,d}/\varepsilon_F^{s,d}\simeq 4d/a_B$. The latter value is about 0.35 and 0.07, respectively, in the cases of SiO_2 and HfO_2 as dielectrics. The parameters d/W and $a_B/4W$ are assumed to be small in the following.

III. DARK CURRENT

The source-drain current (which is a thermionic current by nature) is created by the electrons injected from the source and the drain sections into the gated section over the barrier in the gated section. Taking into account that the electrons in the gated section due to $\Delta^s>\varepsilon_F^s$ and $\Delta^d>\varepsilon_F^d$ are nondegenerate (in contrast to the source and the drain sections) in the range of the top-gate voltages under consideration, the source-drain thermionic current is given by (see also Ref. 15)

$$J=\beta J_m\left[\exp\left(\frac{\varepsilon_F^s-\Delta^s}{k_BT}\right)-\exp\left(\frac{\varepsilon_F^d-\Delta^d}{k_BT}\right)\right]. \tag{4}$$

Here Δ^s and Δ^d are the heights of the potential barriers for electrons from the source and the drain sides, respectively (under weak illumination $\Delta^s\lesssim\Delta_0^s$ and $\Delta^d\lesssim\Delta_0^d$), k_B is the Boltzmann constant, and T is the temperature. The pre-

expontial factor β is the fraction of the injected electrons that passed through the gated section despite their scattering on impurities and acoustic phonons, i.e., the fraction of the electrons not reflected back. Solving the two-dimensional kinetic Boltzmann equation for the electron distribution function in this section,[15] one can obtain $\beta \simeq 1$ in the ballistic regime of the electron transport across the gated section ($\nu\tau \ll 1$ or $L_t \ll \sqrt{2k_BT/m}/\nu$) and $\beta \simeq \sqrt{\pi}/\nu\tau \ll 1$ in the collision-dominated regime ($\nu\tau \gg 1$), where ν is the characteristic frequency of the electron scattering on defects and acoustic phonons in the gated section, $\tau = L_t\sqrt{m/2k_BT}$ is the effective ballistic transit time across the gated section of electrons with the thermal velocity $v_T = \sqrt{2k_BT/m}$, and L_t is the length of the top gate.[15] Another pre-exponential factor J_m is the characteristic current on the thermionic injection, for which one obtains

$$J_m = e\frac{\sqrt{2m}(k_BT)^{3/2}}{\pi^{3/2}\hbar^2}N, \tag{5}$$

where $N=N(T) \lesssim 1$ reflects a deviation (which can be marked in the source and the drain sections but not in the gated section) of the real electron-energy spectrum in the GBL from the parabolic one with the effective mass m. This factor provides some decrease in the dark current. However, it disappears out of the final expressions for the photocurrent and the GBL-PT responsivity derived below.

Using Eqs. (1), (3), and (4), we arrive at the following formula for the source-drain current without illumination (when $\Delta^s = \Delta_0^s$ and $\Delta^d = \Delta_0^d$), i.e., for the so-called GBL-PT dark current:

$$J_0 \simeq \beta J_m \exp\left(\frac{\varepsilon_F^s}{k_BT}\right)\exp\left[\frac{e(V_b+V_t)}{2k_BT}\right]\left[1-\exp\left(-\frac{eV_d}{k_BT}\right)\right]$$
$$= \beta J_m \exp\left[-\frac{e(V_{th}-V_t)}{2k_BT}\right]\left[1-\exp\left(-\frac{eV_d}{k_BT}\right)\right]. \tag{6}$$

As explicitly follows from Eq. (6), the dark current depends on the back- and the top-gate voltages. This dependence originates from the voltage dependences of the barrier heights and the Fermi energies. If for a given value of the back-gate voltage V_b, the top-gate voltage is maintained to be $V_t = V_{th}^*$, and for the source-drain voltage $V_d \gtrsim k_BT/e$, taking into account the smallness of d/W and $a_B/4W$, we find $J_0 = J_0^* \simeq \beta J_m \exp(-E_g/k_BT) \simeq \beta J_m \exp(-dV_b/Wk_BT)$. The case under consideration corresponds to the highest barrier in the gated section at which the interband tunneling can still be neglected (because the Fermi level in the source section is above the top of the valence band in the gated section or aligns with it if $V_{th}^* \leq V_t$). Figure 2 shows the dark current versus the back-gate voltage at $V_t = V_{th}^*$ calculated for different temperatures. It is assumed that $d=0.35$ nm, $W=20$ nm, and $\beta=0.1$. The voltage range considered in Fig. 2 ($V_b=1-4$ V) corresponds to the energy gap in the gated section $E_g \simeq 17-70$ meV.

IV. PHOTOCURRENT AND RESPONSIVITY

As a result of illumination with the photon energy $\hbar\omega > E_g$, the photogenerated holes accumulate in the gated section. Their density Σ can be found from the following equation governing the balance between the photogeneration of holes and their thermionic escape to the source and drain sections:

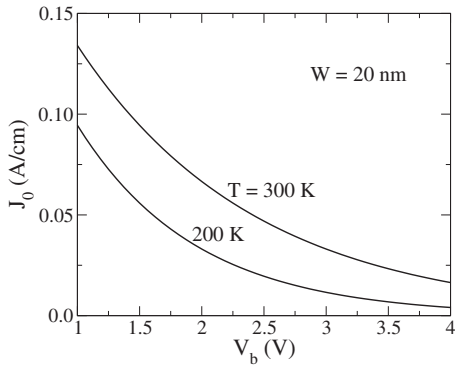

FIG. 2. Dark current J_0 as a function of back-gate voltage V_b (at $V_t = V_{th}^*$) at different temperatures T.

$$\frac{\beta_c J_m}{e}\frac{\Sigma}{\Sigma_t}\exp\left(-\frac{d}{2W}\frac{eV_t}{k_BT}\right)\exp\left[\frac{e(V_b+V_t)}{2k_BT}\right]\left[1+\exp\left(-\frac{eV_d}{k_BT}\right)\right]$$
$$= G_\omega. \tag{7}$$

Here β_c is the fraction of the holes injected from the gated section into the source and the drain sections (i.e., into the contact sections) but not reflected back by the scattering processes (β_c is determined not only by the hole collision frequency in these sections but also by the rate of recombination in these sections and the contacts), $\Sigma_t = 2mk_BT/\pi\hbar^2$, and G_ω is the rate of photogeneration of electrons and holes owing to the absorption of the incident THz/FIR radiation. The left-hand side of Eq. (8) is the hole flux associated with their thermionic escape from the gated section into the source and the drain sections provided the hole density is small (due to weak illumination), so that the hole system in the gated section is far from degeneration. The rate of photogeneration depends on the intensity of radiation I_ω; the absorption quantum efficiencies α_ω, α_ω^s, and α_ω^d in the pertinent sections; and their lengths. The absorption quantum efficiencies in question are given by[17]

$$\alpha_\omega = \left(\frac{\pi e^2}{c\hbar}\right)\left(\frac{\hbar\omega+2\gamma_1}{\hbar\omega+\gamma_1}\right)\Theta(\hbar\omega-E_g), \tag{8}$$

$$\alpha_\omega^{s,d} \simeq \left(\frac{\pi e^2}{c\hbar}\right)\left(\frac{\hbar\omega+2\gamma_1}{\hbar\omega+\gamma_1}\right)\Theta(\hbar\omega-E_g^{s,d})B_\omega, \tag{9}$$

where c is the speed of light and $\Theta(\hbar\omega)$ is a steplike function related to the energy dependence of the density of states including its peculiarity at the energy-gap edges and collisional smearing. The factor B_ω in Eq. (9) reflects the Burstein-Moss effect[18]

$$B_\omega = \left[1+\exp\left(-\frac{\hbar\omega - E_g^{s,d} - 2\varepsilon_F^{s,d}}{2k_BT}\right)\right]^{-1} \times \left[1+\exp\left(-\frac{\hbar\omega + E_g^{s,d} + 2\varepsilon_F^{s,d}}{2k_BT}\right)\right]^{-1} \simeq \left[1+\exp\left(-\frac{\hbar\omega - E_g^{s,d} - 2\varepsilon_F^{s,d}}{2k_BT}\right)\right]^{-1}.$$

For the THz/FIR radiation with $E_g \lesssim \hbar\omega \ll \gamma_1$, Eq. (8) yields $\alpha_\omega \simeq \alpha = 2\pi e^2/c\hbar = 2\pi/137$. However, the absorption coefficient in the source and the drain sections can be rather small due to the Burstein-Moss effect. This occurs if the electron system in these sections is degenerate ($\varepsilon_F^{s,d} \gg k_BT$) and the photon energy does not markedly exceed the energy gap. Indeed, at $\hbar\omega \gtrsim E_g \simeq 2E_g^{s,d}$, considering that $E_g^{s,d}/\varepsilon_F^{s,d} \simeq 4d/a_B < 1$, from Eq. (9) one obtains $\alpha_\omega^{s,d} \simeq \alpha \exp(-\varepsilon_F^{s,d}/k_BT) \ll \alpha$.

Disregarding the absorption of radiation in the source and the drain sections and considering that

$$G_\omega = \frac{L_t \alpha_\omega I_\omega}{\hbar\omega}, \tag{10}$$

Eq. (7) can be presented as

$$\frac{\beta_c J_m}{e}\frac{\Sigma}{\Sigma_t}\exp\left(-\frac{d}{2W}\frac{eV_t}{k_BT}\right)\exp\left[\frac{e(V_b+V_t)}{2k_BT}\right]\left[1+\exp\left(-\frac{eV_d}{k_BT}\right)\right] = L_t\frac{\alpha_\omega I_\omega}{\hbar\omega}. \tag{11}$$

The charge of the photogenerated holes in the gated section lowers of the potential barrier by the value

$$\Delta^{s,d} - \Delta_0^{s,d} = -\frac{4\pi e^2 W}{k}\Sigma. \tag{12}$$

Hence, in the absence of illumination, one obtains $\Delta^{s,d} = \Delta_0^{s,d}$. Considering Eqs. (4), (6), and (12), the variation in the source-drain current under illumination $\Delta J = J - J_0$, i.e., the value of the photocurrent, can be presented by the following formula:

$$\Delta J = J_0 \frac{4\pi e^2 W}{k k_B T}\Sigma. \tag{13}$$

It should be noted that the contribution of the photogenerated electrons to the net photocurrent can be neglected because it is small [see Eq. (18) in Sec. V] and the photogenerated electrons are swept out from the gated section to both the source and the drain sections (virtually in equal portions). Then, using Eqs. (6), (10), and (13), we arrive at

$$\Delta J = e\frac{L_t\beta}{\beta_c}J_m \exp\left(\frac{\varepsilon_F^s}{k_BT}\right)\exp\left(\frac{d}{2W}\frac{eV_t}{k_BT}\right) \times \left[\frac{1-\exp(-eV_d/k_BT)}{1+\exp(-eV_d/k_BT)}\right]\frac{\alpha_\omega I_\omega}{\hbar\omega}. \tag{14}$$

Using Eq. (14), the GBL-PT responsivity defined as $R_\omega = \Delta J/(L_t+2L_c)I_\omega$, where L_t+2L_c is the net length of the GBL channel (the lengths of the source and the drain sections are assumed to be equal to each other: $L_s = L_d = L_c$) can be presented as

$$R_\omega = \frac{e\alpha C}{\hbar\omega}\left(\frac{8W}{a_B}\right)\Theta\left[\hbar\omega - \frac{ed(V_b - V_t)}{2W}\right]\exp\left(\frac{\varepsilon_F^s}{k_BT}\right) \times \exp\left(\frac{d}{2W}\frac{eV_t}{k_BT}\right)\left[\frac{1-\exp(-eV_d/k_BT)}{1+\exp(-eV_d/k_BT)}\right]. \tag{15}$$

Here, $C = L_t\beta/(L_t+2L_c)\beta_c$ is the collision factor. At $\hbar\omega = 10$ meV and $C = 1$, one obtains $R_\omega = (e\alpha C/\hbar\omega) \simeq 4.6$ A/W.

At $V_t = V_{th}^*$ and $eV_d > k_BT$, Eq. (15) can be reduced to the following:

$$R_\omega \simeq \frac{e\alpha C}{\hbar\omega}\left(\frac{8W}{a_B}\right)\Theta(\hbar\omega - \hbar\omega_{off})\exp\left[\left(\frac{\varepsilon_F^s}{k_BT}\right)\left(1-\frac{4d}{a_B}\right)\right]. \tag{16}$$

Here $\hbar\omega_{off} = E_g \simeq ed(V_b - V_t)/2W \gtrsim edV_b/W$ is the photon cutoff energy. At $\hbar\omega_{off} \gtrsim E_g$, the GBL-PT responsivity reaches a maximum,

$$\max R_\omega \simeq \frac{\alpha C}{V_b}\left(\frac{8W^2}{da_B}\right)\left[\exp\left(\frac{\varepsilon_F^s}{k_BT}\right)\left(1-\frac{4d}{a_B}\right)\right]. \tag{17}$$

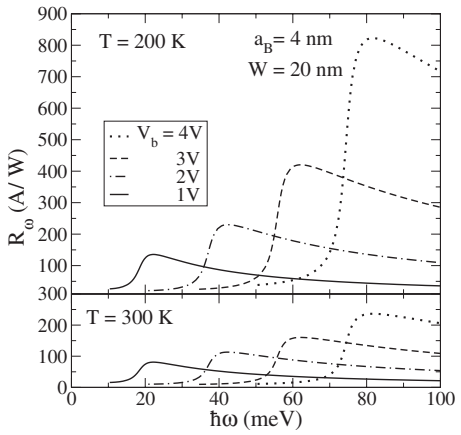

FIG. 3. GBL-PT responsivity R_ω versus photon energy $\hbar\omega$ for different back-gate voltages V_b at different temperatures T.

Figure 3 shows the GBL-PT responsivity R_ω as a function of the photon energy $\hbar\omega$ calculated using Eq. (16) for different back-gate voltages V_b at different temperatures. Here and in the following figures, it is set that for each value of the back-gate voltage V_b, the top-gate voltage is chosen to be $V_t = V_{th}^*$. The source-drain voltage is assumed to be $V_d > k_BT/e$. Taking into account some smearing γ of the absorption edge and disregarding the peculiarity of the density of states at the energy-gap edges, we set $\Theta(\hbar\omega) = [1/2 + (1/\pi)\tan^{-1}(\hbar\omega/\gamma)]$. We set $d = 0.35$ nm, $a_B = 4$ nm, $W = 20$ nm, $\gamma = 2$ meV, $\beta = 0.1$, and $C = 1$. As seen from Fig. 3, the GBL-PT spectral characteristics can be effectively tuned by the applied voltages.

According to Eq. (17), the dependence of the responsivity maximum value $\max R_\omega$ on the back-gate voltage V_b is associated with the variation ε_F^s with varying V_b. The ε_F^s versus V_b relationship is determined by the energy dependence of

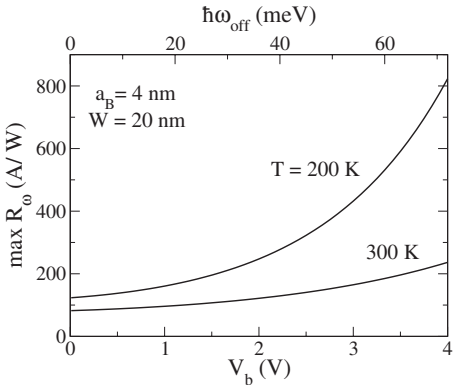

FIG. 4. Dependences of maximum GBL-PT responsivity on the back-gate voltage (cutoff photon energy $\hbar\omega_{off}$) at different temperatures T.

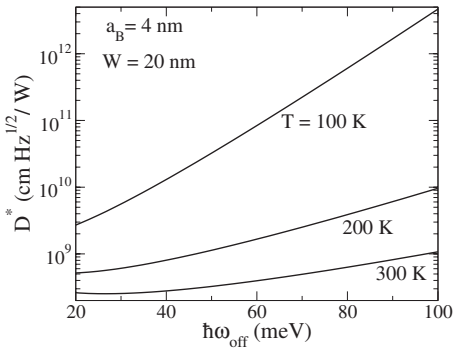

FIG. 5. GBL-PT dark-current-limited detectivity D^* versus cutoff photon energy $\hbar\omega_{off}$ at optimized gate voltages V_b and V_t and different temperatures T.

the GBL density of states. For simplified calculations one can assume that the density of states as a function of the energy is constant. In this case, as indicated in Sec. II, $\varepsilon_F^s \simeq (a_B/8W)eV_b$ [and $\varepsilon_F^d \simeq (a_B/8W)e(V_b - V_d)$]. Figure 4 shows the dependences of the responsivity maximum value max R_ω on the back-gate voltage V_b (and the photon energy $\hbar\omega_{off}$) calculated using Eq. (17) under the above assumption for the same parameters as in Fig. 3. As seen from Fig. 4, max R_ω steeply increases with increasing V_b: $\ln(\max R_\omega) \propto V_b/T$. However, since a linear increase in the density of states as a function of the energy in the range of elevated energies becomes essential, the dependences of ε_F^s and ε_F^d on V_b in the range of large V_b can be more complex: $\varepsilon_F^s \propto [\sqrt{1+AV_b}-1]$ and $\varepsilon_F^s \propto [\sqrt{1+A(V_b-V_d)}-1]$, respectively. Here A is a parameter of the GBL energy-band structure. Hence, at a moderate V_b, $\varepsilon_F^s \propto AV_b$ and $\varepsilon_F^s \propto A(V_b-d)$ (as above), while at elevated values of V_b, one obtains $\varepsilon_F^s \propto \sqrt{AV_b}$ and $\varepsilon_F^d \propto \sqrt{A(V_b-V_d)}$. This results in more complex voltage dependences of $\ln(\max R_\omega)$ in the range of elevated V_b than those shown in Fig. 4.

V. PHOTOELECTRIC GAIN AND DETECTIVITY

Considering Eq. (14) and taking into account that the photocurrent created by the photogenerated electrons and holes can be estimated as $\Delta J_0 = eL_t\alpha_\omega I_\omega/\hbar\omega$, the photoelectric gain $g = \Delta J/\Delta J_0$ can be presented as

$$g \simeq \frac{\beta}{\beta_c}\exp\left[\left(\frac{\varepsilon_F^s}{k_BT}\right)\left(1-\frac{4d}{a_B}\right)\right], \tag{18}$$

where all the factors in the right-hand side exceed or greatly exceed unity. Hence, g, i.e., the ratio of the net photocurrent (which is mainly the injected current stimulated by the barrier lowering due to illumination and accumulation of hole) and the current of the photogenerated electrons and holes, substantially exceeds unity [this was used in deriving of Eq. (14)]. The above expression for ΔJ_0 assumes that all electrons photogenerated in the gated section go to the drain due to asymmetry of the barrier caused by the source-drain bias, while almost all photogenerated holes are captured in this section. In reality, some portions of the photogenerated electrons can escape from the gate section into the source. As a result, ΔJ_0 can be somewhat smaller than the above estimate, leading to even higher photoelectric gain than that given by Eq. (18). Assuming that all the GBL-PT sections are so long ($L_c \gg v_T/\nu_c$ and $L \gg v_T/\nu$) that the electron transport in all of them is collision dominated and setting for definiteness $\nu_c = \nu$ and $L_c = L_t/2$, one can obtain $\beta/\beta_c = 2$. Roughly estimating the Fermi energy as $\varepsilon_F^s \simeq (a_B/8W)eV_b \simeq 0.2$ eV (for $a_B = 4$ nm, $W = 20$ nm, and $V_b = 1-2$ V) for $T = 300$ K, we arrive at $g \simeq 27-360$.

Calculating the GBL-PT dark-current-limited detectivity, which by definition is the signal-to-noise ratio appropriately normalized by the detector area and the measurement electrical bandwidth,[1–3] as $D^* = R_\omega/\sqrt{4egJ_0/H}$, where H is the GBL-PT width (in the direction perpendicular to the current), at properly chosen relationship between V_b and V_t (as above), we arrive at the following formula:

$$D^* \simeq \frac{e\alpha C^*}{\hbar\omega_{off}}\sqrt{\frac{H}{4eJ_m}}\sqrt{\frac{8W}{a_B}}\exp\left(\frac{\hbar\omega_{off}}{nk_BT}\right), \tag{19}$$

where $C^* = C\sqrt{\beta_c}/\beta = [L_t/(L_t+2L_c)\sqrt{\beta_c}]$ and $n = 2/(1+\varepsilon_F^s/E_g)$. Estimating $E_g/\varepsilon_F^s \simeq 8d/a_B$, we obtain $n = (16d/a_B)/(1+8d/a_B)$. A point worth noting is that the factor n in the exponential dependence in Eq. (19) can be about or smaller than unity. Indeed, for $a_B = 4-20$ nm, one obtains $n \simeq 0.25-0.82$. This provides a fairly steep increase in D^* with increasing $\hbar\omega_{off}$ or a relatively slow decrease in D^* with increasing T.

Figures 5 and 6 demonstrate the dark-current-limited detectivity D^* (at $V_t = V_{th}^*$) as a function of the cutoff photon energy $\hbar\omega_{off}$ at different temperatures T and as a function of T at given values of $\hbar\omega_{off}$. One can see that D^* can be fairly large even at room temperatures. The detectivity becomes modest at low cutoff photon energies. However, as shown in Fig. 7, in GBL-PTs with relatively high-k gate layers in which the Bohr radius can be large, a rather high detectivity can be achieved in the range of low cutoff photon energies, in particular, those corresponding to the THz range of spectrum.

VI. COMMENTS

A. Comparison with other detectors

As follows from Eqs. (15)–(19) and demonstrated in Figs. 3–7, the GBL-PT responsivity and detectivity can be very

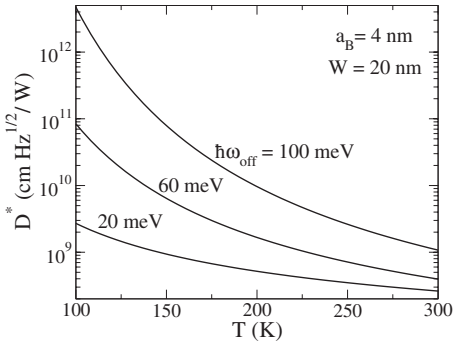

FIG. 6. Temperature dependences of GBL-PT dark-current-limited detectivity D^* for different cutoff photon energies $\hbar\omega_{off}$.

large even at room temperatures exceeding those of QWIP and QDIPs. This is attributed to the following. First of all, the quantum efficiency of the interband absorption α is relatively large (in comparison, say, with the intersubband transitions in single QWIPs). Indeed, $\alpha=2\pi/137\simeq 4.6\times10^{-2}$, while the QWIP quantum efficiency $\alpha^{(\mathrm{QW})}=\sigma^{(\mathrm{QW})}\Sigma^{(\mathrm{QW})}\simeq 2\times10^{-3}$ (for the typical values of the cross section of photon absorption in a QW due to the interband transition $\sigma^{(\mathrm{QW})}=2\times10^{-15}$ cm^2 and the donor concentration in a QW $\Sigma^{(\mathrm{QW})}=10^{12}$ cm^{-2}). Second, as shown above, the photoelectric gain exhibited by GBL-PTs can also be very large (from several tens to several hundreds, whereas in QWIPs, $g\sim10^3$). This is associated with a higher energy barrier (high activation energy) for the photogenerated holes accumulated in the gated section in comparison with the activation energies for electrons in the source and the drain sections. The difference between the activation energies is equal to $\varepsilon_F^{s,d}-E_g+E_g^{g,s}\simeq(a_B/8W)(1-4d/a_B)eV_b$. An increase in the gate-voltages results in an increase in the Fermi energy of electrons in the source and the drain sections and in a rise of the activation energy for the photogenerated holes leading to an increase in their lifetime. As a result, the temperature dependence of the GBL-PT detectivity is given by the factor $\exp(\hbar\omega_{off}/nk_BT)$ with $n<2$ in contrast to QWIPs (optimized) for which $D^*\propto\exp(\hbar\omega_{off}/2k_BT)$ (see, for instance, Ref. 4). In particular, for QWIPs $\hbar\omega_{off}=60$ meV at $T=100$ K, $D^*\sim10^8$ cm Hz$^{1/2}$/W (Refs. 1 and 3) (compare with the value $D^*\sim10^{11}$ cm Hz$^{1/2}$/W for a GBL-PT in Fig. 6, which somewhat exceeds that of HgCdTe photodiodes[1]). Since even at relatively high temperatures GBL-PTs can exhibit fairly high detectivity, there are good prospects to use GBL-PTs as THz/FIR photodetectors operating at elevated temperatures. The dependence of the cutoff photon energy on the applied voltages ($\bar{\omega}_{off}\propto V_b$ at properly chosen V_t) opens up prospects of the development of GBL-PT-based detectors with voltage-tuned spectral characteristics and multicolor detector arrays.

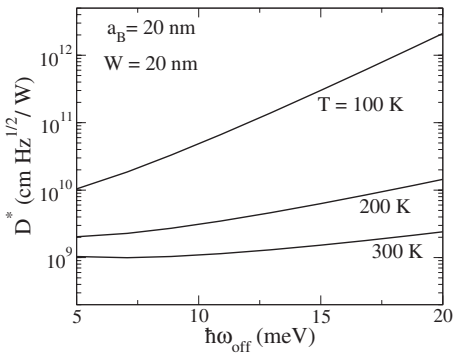

FIG. 7. The same as in Fig. 5 but for GBL-PT with different value of the Bohr radius a_B (different dielectric constant of gate layers k).

B. Role of interband tunneling

The GBL-PT responsivity and detectivity can be limited by the interband tunneling of the photogenerated holes. This can deteriorate the GBL-PT performance due to an increase in the dark current and a decrease in the photoelectric gain associated with a shortening of the lifetime of the photogenerated holes. If $V_{th}^*\lesssim V_t$, the Fermi level in the source section corresponds to the energy gap in the gated section [this Fermi level lies higher than the top of the valence band in the gated section as shown in Fig. 1(b)], so that the interband tunneling from the conduction band in the former section to the valence band of the latter section is effectively suppressed. Similar situation occurs in the junction between the gated and the drain sections (see also below). If $V_t<V_{th}^*$, the interband tunneling in question can be essential if the width of the junction between the source (or drain) and the gated sections W^* is too small (W^* depends on W as well as on V_b and V_t). At $V_t\lesssim V_{th}^*$, the interband tunneling in the junction between the source and the gated sections can be disregarded if the tunneling current is small in comparison with the thermionic current above the barrier. Estimating the probability of interband tunneling as[19] $\exp(-\pi m^{1/2}E_g^{3/2}/2\sqrt{2}e\hbar\mathcal{E})$, where $\mathcal{E}\simeq E_g/eW^*$, we obtain the inequality $\exp(-\pi m^{1/2}E_g^{3/2}/2\sqrt{2}e\hbar\mathcal{E})\ll\exp(-E_g/k_BT)$ and arrive at the following condition when the tunneling of the photogenerated holes should not be essential:

$$W^*>\frac{2\sqrt{2}\hbar}{\pi\sqrt{m}}\frac{\sqrt{\hbar\omega_{off}}}{k_BT}. \tag{20}$$

For instance, for $\hbar\omega_{off}=100$ meV and $T=300$ K and for $\hbar\omega_{off}=100$ meV and $T=30$ K, inequality (20) yields $W^*>15$ nm and $W^*>50$ nm, respectively.

In the case of a large source-drain voltage V_d, the interband tunneling (which can be suppressed in the junction between the source and the gated sections as discussed above) can become essential in the drain junction resulting in marked dark current. This can also substantially deteriorate the GBL-PT performance. To avoid this, the tunneling current through the drain junction should not be too strong in comparison with that through the source junction. This occurs when the source-drain voltage V_d is kept sufficiently low (at least not exceeding too much the value k_BT/e). Considering that the photocurrent ΔJ as a function of V_d at $V_d\gtrsim k_BT/e$ saturates [see Eq. (14)], for the optimal source-drain bias in the range of temperatures under consideration one obtains $V_d\simeq25-30$ mV.

C. Collision factor

The collision factor C in Eqs. (15)–(17) can influence the GBL-PT performance. It depends on the device geometrical parameters L_t and L_c. Since the propagation of holes in the source and the drain sections can be strongly affected by scattering on electrons due to their large density, the hole collision frequency in the source and the drain sections $\nu_c > \nu$ (or even $\nu_c \gg \nu$). In such a case, C can markedly exceed unity. This is because strong collisions of holes in the source and the drain sections can essentially decrease the current of the photogenerated holes from the gated section into the source section (as well as into the drain section) increasing the holes lifetime and, hence, the photoelectric gain. To follow the dependence of C (and, consequently, R_ω) on L_t and L_c, assuming that the holes recombine primarily at the contacts, one can use the following interpolation formulas: $\beta_c = [1+(\nu_c L_c/v_T)^2/\pi]^{-1/2}$ and $\beta = [1+(\nu L_t/v_T)^2/\pi]^{-1/2}$. As a result, we obtain

$$C \simeq \frac{L_t}{(L_t+2L_c)} \sqrt{\frac{1+(\nu_c L_c/v_T)^2/\pi}{1+(\nu L_t/v_T)^2/\pi}}. \tag{21}$$

As follows from Eq. (21), C as a function of L_t exhibits a maximum at a certain value of the latter. If both L_c and L_t are large, so that the electron transport in all the sections is collision dominated, $C \simeq [L_c/(L_t+2L_c)](\nu_c/\nu)$.

D. Absorption in the source and the gate sections

When the photon energy $\hbar\omega \gtrsim E_g^{s,d}+2\varepsilon_F^{s,d}$, the radiation absorption in the source and the drain sections can be essential. In such a spectral range, the holes photogenerated in these sections can substantially affect the net hole charge in the gated section (and increase the quantum efficiency). In this case, the quantity G_ω in the right-hand side of Eq. (7) should be modified to take into account the extra holes photogenerated in the source and the drain sections and injected into the gated section. The contribution of the holes photogenerated in the source and the drain sections can result in a modification in the spectral characteristic of the responsivity at elevated photon energies according to the spectral dependence of the factor B_ω in Eq. (9). As a result, a duplicated maxima of R_ω can appear which correspond to $\hbar\omega \simeq \hbar\omega_{off} \gtrsim edV_b/W$ and $\hbar\omega \simeq \hbar\omega_{off}/2+2\varepsilon_F^s \simeq (edV_b/W)(1+a_B/4d)/2 \simeq 1.9\hbar\omega_{off}$ (at $a_B=4$ nm).

E. Multiple GBL-PT structures

We considered a GBL-PT with the structure of a single field-effect transistor. Actually, analogous GBL photodetectors can be made of multiple periodic GBL-PT structures. Such photodetectors can surpass the GBL-PT considered above. However, their operation can be complicated by additional features of the photogenerated holes transport. As a result, the potential distribution along the GBL channel can be nontrivial as it takes place in multiple QWIPs (see, for instance, Refs. 20 and 21), so that special studies of multiple GBL-PTs are required.

F. Main assumptions

Let us summarize the main assumptions of the model under consideration. Our model is based on the rather standard equation [Eq. (4)] for the calculations of the terminal current in the field-effect and bipolar transistors operating as phototransistors in the regime of the photosensitive barrier which controls the electron injection. The features of the model are (i) unusual for customary devices dependences of the energy gaps in different sections on the back- and the top-gate voltages; these dependences were assumed linear [see Eq. (2)] in line with the previous publications of other authors;[11,13,16] (ii) specific spectral dependences of the interband absorption quantum efficiencies in the form of Eqs. (8) and (9) (Ref. 17); (iii) neglecting of the interband tunneling in the junctions between the source and the gated sections and between the gated and the drain sections. As discussed in Sec. VI, this can be justified if the structure geometrical parameters and the bias voltages are chosen properly; and (iv) the expressions for such characteristics as the photocurrent, responsivity, photoelectric gain, and detectivity are explicitly expressed via the electron Fermi energy in the source section. This Fermi energy depends on the back-gate voltage. Such a dependence is determined by the energy dependence of the density of state. To obtain the explicit voltage dependences of the GBL-PT characteristics and in some estimates, we used a simplified relation between the Fermi energy and the back-gate voltage, which corresponds to a constant density of states, although the effect of the density of states increasing with the energy is pointed out as well. Certainly, for the optimization of real GBL-PTs, particularly those with high-k dielectric layers operating at elevated voltages in which the Fermi energy band be fairly large, more strict calculations of the ε_F^s versus V_b relation might be indispensable in future.

VII. CONCLUSIONS

We proposed a GBL-PT and calculated its spectral characteristics, dark current, responsivity, photoelectric gain, and dark-current-limited detectivity. It was shown that GBL-PTs with optimized structure at properly chosen applied voltages can surpass the photodetectors of other types. The main advantages of GBL-PTs are associated with the utilization of interband transitions with relatively high quantum efficiency, high photoelectric gain, and with the possibility of operation at elevated temperatures. Additional advantages of the GBL-PTs with respect to QWIPs, QDIPs, and QRIPs, as well as to HgCdTe and InSb detectors, include easy fabrication and integration with silicon (or graphene) readout circuits and voltage tuning of the spectral characteristics.

ACKNOWLEDGMENTS

The authors are grateful to S. Brazovskii, N. Kirova, V. Mitin, T. Otsuji, and E. Sano for useful discussions and to T. Orr for comments on the manuscript. The work was supported by the Japan Science and Technology Agency, CREST, Japan.

*v-ryzhii@u-aizu.ac.jp

[1] A. Rogalski, in *Intersubband Infrared Photodetectors*, edited by V. Ryzhii (World Scientific, Singapore, 2003), p. 1.
[2] K. K. Choi, *The Physics of Quantum Well Infrared Photodetectors* (World Scientific, Singapore, 1997).
[3] H. Schneider and H. C. Liu, *Quantum Well Infrared Photodetectors* (Springer, Berlin, 2007).
[4] V. Ryzhii, Semicond. Sci. Technol. **11**, 759 (1996).
[5] V. Ryzhii, I. Khmyrova, M. Ryzhii, and M. Ershov, J. Phys. IV **06**, C3-157 (1996).
[6] C. Berger, Z. Song, T. Li, X. Li, A. Y. Ogbazhi, R. Feng, Z. Dai, A. N. Marchenkov, E. H. Conrad, P. N. First, and W. A. de Heer, J. Phys. Chem. **108**, 19912 (2004).
[7] K. S. Novoselov, A. K. Geim, S. V. Morozov, D. Jiang, M. I. Katsnelson, I. V. Grigorieva, S. V. Dubonos, and A. A. Firsov, Nature (London) **438**, 197 (2005).
[8] B. Obradovic, R. Kotlyar, F. Heinz, P. Matagne, T. Rakshit, M. D. Giles, M. A. Stettler, and D. E. Nikonov, Appl. Phys. Lett. **88**, 142102 (2006).
[9] Z. Chen, Y.-M. Lin, M. J. Rooks, and P. Avouris, Physica E (Amsterdam) **40**, 228 (2007).
[10] T. Ohta, A. Bostwick, T. Seyel, K. Horn, and E. Rotenberg, Science **313**, 951 (2006).
[11] E. McCann, Phys. Rev. B **74**, 161403(R) (2006).
[12] E. McCann and V. I. Fal'ko, Phys. Rev. Lett. **96**, 086805 (2006).
[13] E. V. Castro, K. S. Novoselov, S. V. Morozov, N. M. R. Peres, J. M. B. Lopes dos Santos, J. Nilsson, F. Guinea, A. K. Geim, and A. H. Castro Neto, Phys. Rev. Lett. **99**, 216802 (2007).
[14] V. Ryzhii, V. Mitin, M. Ryzhii, N. Ryabova, and T. Otsuji, Appl. Phys. Express **1**, 063002 (2008).
[15] V. Ryzhii, M. Ryzhii, A. Satou, T. Otsuji, and N. Kirova, J. Appl. Phys. **105**, 104510 (2009).
[16] E. V. Castro, K. S. Novoselov, S. V. Morozov, N. M. R. Peres, J. M. L. dos Santos, J. Nilsson, F. Guinea, A. K. Geim, and A. H. Castro Neto, arXiv:0807.3348 (unpublished).
[17] V. Ya. Aleshkin, A. A. Dubinov, and V. Ryzhii, JETP Lett. **89**, 63 (2009).
[18] J. I. Pankove, *Optical Processes in Semiconductors* (Dover Publications, New York, 1971).
[19] S. M. Sze, *Physics of Semiconductor Devices* (Wiley, New York, 1981).
[20] V. Ryzhii and H. C. Liu, Jpn. J. Appl. Phys., Part 1 **38**, 5815 (1999).
[21] V. Ryzhii, M. Ryzhii, and H. C. Liu, J. Appl. Phys. **91**, 5887 (2002).